Article

3D CPFD Simulation of Circulating Fluidized Bed Downer and Riser: Comparisons of Flow Structure and Solids Back-Mixing Behavior

Yancong Liu, Yingya Wu, Xiaogang Shi, Chengxiu Wang, Jinsen Gao and Xingying Lan *

State Key Laboratory of Heavy Oil Processing, China University of Petroleum, Beijing 102249, China; yancong_liu@outlook.com (Y.L.); yaya0224@live.com (Y.W.); shixiaogang68@cup.edu.cn (X.S.); cwang1277@cup.edu.cn (C.W.); jsgao@cup.edu.cn (J.G.)

* Correspondence: lanxy@cup.edu.cn; Tel.: +86-1861-096-2527

Abstract: The difference of gas-solids flow between a circulating fluidized bed (CFB) downer and riser was compared by computational particle fluid dynamics (CPFD) approach. The comparison was conducted under the same operating conditions. Simulation results demonstrated that the downer showed much more uniform solids holdup and solids velocity distribution compared with the riser. The radial non-uniformity index of the solids holdup in the riser was over 10 times than that in the downer. In addition, small clusters tended to be present in the whole downer, large clusters tended to be present near the wall in riser. It was found that the different cluster behavior is important in determining the different flow behaviors of solids in the downer and riser. While the particle residence time increased evenly along the downward direction in the downer, particles with both shorter and longer residence time were predicted in the whole riser. The nearly vertical cumulative residence time distribution (RTD) curve in the downer further demonstrated that the solids back-mixing in the downer is limited while that in the riser is severe. Solids turbulence in the downer was much weaker compared with the riser, while the large clusters formation near the wall in the riser would hinder solids transportation ability.

Keywords: gas-solids flow; downer; riser; back-mixing; CPFD

1. Introduction

The circulating fluidized bed (CFB) [1], which is extensively applied in industrial production such as fluidized catalytic cracking (FCC) and coal combustion [2], is mainly composed of a riser in which the gas phases move upward and the solids phases move upward in the center and flow downward at the wall, as well as composed of a downer in which the gas-solids phases flow downward co-currently. CFB risers show various advantages including good gas-solids contact efficiency and high gas-solids throughput [3]. However, CFB risers still have some limitations such as severe solids back-mixing and clustering, which will reduce the gas-solids contact and could be detrimental to the reaction selectivity [4]. Compared to the conventional riser, the downer as a type of novel reactor shows rather uniform flow structure and less solids back-mixing [5], which is conductive to the reaction requiring short contact time at high temperature [6]. For instance, the downer reactor is suitable for the coal pyrolysis reaction [7] and fluidized catalytic cracking reaction [8]. Therefore, the downer has drawn increasingly more attention in the past decade. Plenty of scholars have paid attention to the hydrodynamics [9–12], heat transfer [13], and mass transfer [14], as well as the chemical reactions [15] experimentally in the downer.

From the other side, the coal combustion reaction which happens in the CFB riser (boiler) is highly dependent on the sufficient contact between gas (oxygen) and solids (coal particles) in order to

achieve the complete combustion of coal [2]. Hence, much more intense solids back-mixing in the CFB riser is preferred for this type of reaction. From the above mentioned discussion, direct systematic comparisons of downer and riser under the same operating condition and in the same CFB system can provide more information on the performance of the two reactors.

Some experimental studies had been conducted to understand the differences between the downer and riser. Zhang et al. [3] compared different flow behaviors between the downer and riser based on measurement of the radial distribution of the solids holdup and solids velocity with an optic fiber probe. They found that the flow structure in the downer was more uniform than that in the riser, including more uniform radial distribution of solids holdup and velocity, shorter length of flow development, and more uniform axial flow structure. Wang et al. [16] studied the difference of flow development between the downer and riser under high density operation, where the solids circulation rate was up to 700 kg/(m^2·s). They found that the flow behaviors in the downer were still more uniform than that in the riser under high density operation. Ma and Zhu [17] used the heat transfer coefficient measured by miniature heat transfer probe to characterize the different local heat transfer performance between downer and riser. They found that the heat transfer coefficient of the downer were only slightly lower than that of riser in the fully developed region under the same operating conditions. Wang et al. [18] used the ozone decomposition to evaluate the different reaction performance between the downer and riser, and they concluded that the ozone concentration distribution was closely related to the solids holdup, indicating that the different gas-solids flow behavior in the downer and riser had significant influence on the reaction performance of the downer and riser. Overall, the above experimental studies summarized that the gas-solids flow behaviors in the downer was much more uniform compared to the riser, not only under low density operation but also under high density operation. In addition, these previous experimental studies indicated that the heat transfer and reaction performance in the downer and riser were closely associated with the corresponding gas-solids flow characteristics. Comprehensive understanding of the difference of flow characteristics in the downer and riser was critical in analyzing the different heat transfer and reaction performances of the two reactors. However, the experimental measurements are limited in revealing the transient flow behaviors in the downer and riser.

With the development of computing power and multi-phase flow algorithms, computational fluid dynamics (CFD) has become an efficient tool to investigate the local and global gas-solids flow behavior in downer [19,20] and riser [21,22]. The most commonly used CFD approaches include the two-fluid model (TFM), which is based on the Eulerian–Eulerian frame, and the discrete element method (DEM), which is based on the Eulerian–Lagrangian frame. Compared to the TFM, the DEM is able to track the trajectory of each individual particle by solving the Newton's equation on each individual particle. Some scholars have tried to reveal the difference of flow characteristics in downer and riser using the CFD-DEM method. Zhang et al. [23] adopted DEM to study the difference of cluster characteristics such as the local position of cluster, the cluster duration time and cluster velocity in the downer and riser. Zhao et al. [24] employed the CFD-DEM method to find the different residence time distribution of solids in downer and riser, which was obtained by directly tracking the motion of individual particles. However, the traditional Eulerian–Lagrangian approach, such as the DEM, is computationally consuming, which cannot be applied to the simulation of industrial-scale circulating fluidized bed system containing billions of particles.

Computational particle fluid dynamics (CPFD) is a new type of Eulerian–Lagrangian approach [25], which is adopted to overcome the limitations of TFM and DEM, and it is based on the multi-phase particle in cell (MP-PIC) method. In CPFD scheme, particle interactions are described as spatial gradient and particles with the same properties are defined as a parcel. Then the overall flow behavior can be described through tracking the motion of each individual parcel. Therefore, the CPFD approach can extremely reduce the computational cost and it can be applied to the simulation of a pilot-scale and even an industrial-scale CFB system. Additionally, it is able to reveal the detailed information of each single particle visually such as the position of all particles in the bed as well as the velocity

and residence time of each particle. Currently, considerable efforts have been devoted to simulate the CFB downer and riser by using CPFD approach. Lanza et al. [26,27] presented studies to predict the flow behaviors in the developed flow region of a downer using CPFD approach. Wu et al. [28] established a CPFD model coupled with EMMS-based drag model and predicted the flow behavior of a pilot-scale CFB riser handling Geldart A particles and of an industrial-scale FCC riser with a 14-lump kinetic model. Shi et al. [29] investigated the solids residence time distribution and solids back-mixing behavior of a CFB riser by adopting CPFD approach and their results demonstrated that the CPFD approach was capable to obtain the residence time of each individual particle in a pilot-scale riser. With CPFD approach, the previous studies of the authors' research group [28,30] succeeded in describing the flow behavior of CFB downer and riser respectively by considering the cluster effects on the interphase drag force. However, the above mentioned CPFD studies were all based on CPFD approach to simulate the individual downer or riser. Systematic analysis on comparing the difference of gas-solids flow characteristics between the downer and riser is still seldom reported.

In the present work, the CPFD approach incorporated with cluster-based drag model and EMMS-based drag model was adopted to simulate a pilot-scale downer and riser respectively with Geldart A particle in the same CFB system at the same superficial gas velocity and solids circulating flux. The difference of solids holdup as well as some particle-scale information including solids velocity, solids residence time, solids dispersion, and granular temperature between the downer and riser was compared by CPFD approach in order to further analyze the difference of macro-flow behaviors, cluster behaviors, and solids back-mixing. This work is of great significance to provide basic knowledge about the design and operation of the two reactors.

2. CPFD Model and Set-Up

2.1. Simulated CFB System

The downer and riser simulated in this work was from the cold-flow CFB set-up by Wang [31] at Western Ontario University. Figure 1 shows the schematic diagram of the simulated gas-solids CFB system and the 3D computational domain of the CFB downer and riser. In the experimental system, there is one riser with an inner diameter of 0.076 m and a height of 10 m, as well as two downers with an inner diameter of 0.05 m and a height of 4.9 m and an inner diameter of 0.076 m and height of 5.8 m, respectively. The simulation work was conducted in a downer with a height of 5.8 m and an inner diameter of 0.076 m as well as the above mentioned riser. In this work, the downer and riser were under the same superficial velocity of 7 m/s and the same solids circulating flux 200 kg/(m^2·s) were studied respectively. The particles in the downer and riser are FCC particles with a mean diameter of 76 μm and a density of 1780 kg/m^3. For the downer, the gas and particles were fed into the downer from the top inlet and flowed out of the system from the bottom outlet. For the riser, the gas phase was introduced into the main tube with a diameter of 0.076 m continuously and uniformly from the bottom inlet, while a small amount of aeration gas (air) was used to help the particles enter the riser from the storage tank, as well as particles that were fed into the system from the bottom side tube which was vertical to the main tube with a diameter of 0.05 m. During the simulation, we modified the solids inlet angle to make the particles be transported to the outlet smoothly by the gas phase. The gas-solids phase left the riser from the top outlet. The specific parameters of operating conditions are shown in Table 1.
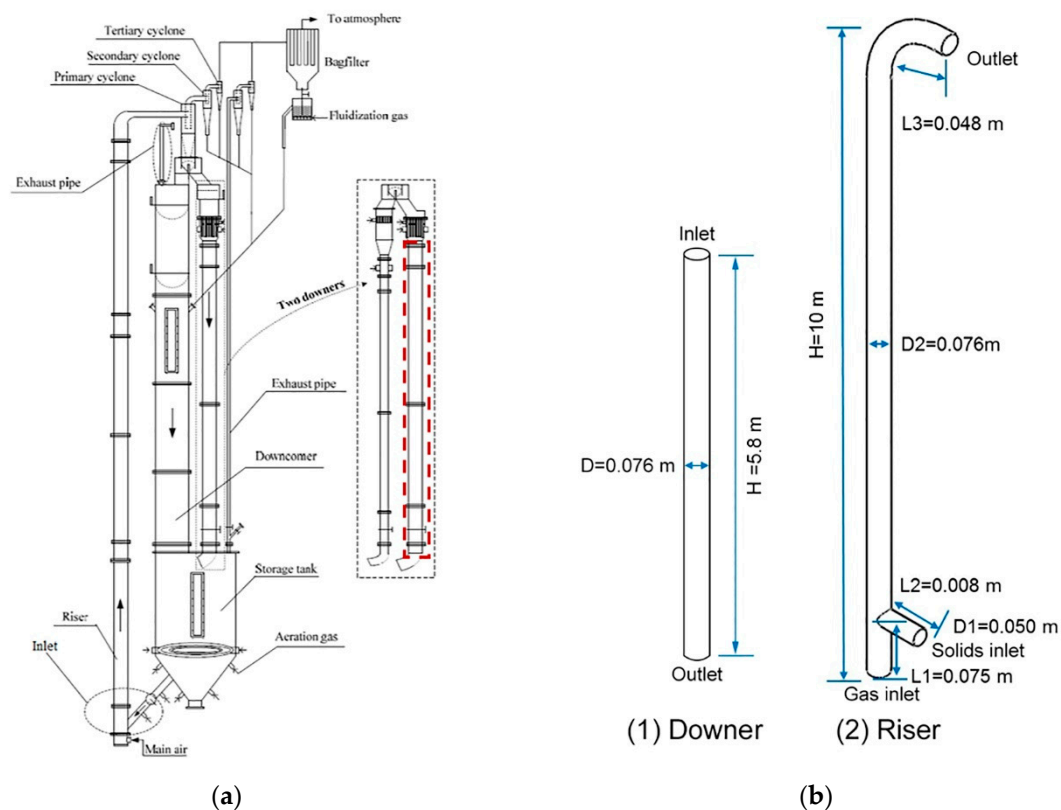
(a)

(b)

Figure 1. Schematic diagram of gas-solids CFB system and the 3D computation domain. (**a**) Experimental apparatus; (**b**) 3D simulated domain of the downer and riser.

Table 1. Operating conditions and modeling parameters of downer and riser.

Item	Downer	Riser
Particle diameter/μm	76	76
Particle density/kg m^{-3}	1780	1780
Solids flux/kg m^{-2} s^{-1}	200	200
Gas viscosity/Pa s	1.84×10^{-5}	1.84×10^{-5}
Gas density/ kg m^{-3}	1.17	1.17
Inlet gas velocity/m s^{-1}	7	7
Bed diameter/m	0.076	0.076
Bed height/m	5.8	10
Packing limit	0.6	0.6
Normal-to-wall momentum retention	0.3	0.3
Tangent-to-wall momentum retention	0.9	0.99
Simulation time/s	20	20
Initial time step/s	5×10^{-4}	5×10^{-4}
Pressure at inlet/Pa	101,300	101,300
Grid number *, $N_x \times N_y \times N_z$	$21 \times 21 \times 900$	$23 \times 17 \times 425$

* The grid number means that the three-dimensional simulated domain was discretized with a uniform grid size in each direction.

2.2. CPFD Model

The 3D CPFD model was used to simulate the above CFB downer and riser. In the CPFD solution process, the fluid phase is described by solving the continuity and momentum equation, and the momentum transfer of particles is described based on the MP-PIC formulation. The governing equations of gas and particles are shown in Table 2. For the simulation of gas-solids CFB system, it is critical to describe the interphase drag force exactly because it has dominant influence on the

predicted flow behaviors. Although the particle concentration in thedowner is low, the clustering effects on the interphase drag force are still needed to be considered in the simulation, and some researches [7,20,32–34] have predicted the flow behaviors in the downer based on the drag model considering the effect of the cluster. In this work, a cluster-based drag model, which was developed by Wu et al. [30] considering the dynamic equilibrium of particles in and out of the cluster, and was used to simulate the CFB downer. On the other hand, the EMMS-based drag model, considering the effects of local heterogeneous structure, have been proven to predict the flow structures in CFB risers more accurately than the conventional homogeneous drag model (e.g., Wen and Yu or Gidaspow drag model) in previous studies [28,35,36]. Therefore, the EMMS-based drag model was selected to simulate the CFB riser. The relevant mathematical equations of the cluster-based drag force model and the EMMS-based drag force model adopted to simulate the downer and riser are shown in Table 3. The detailed calculation procedure of the cluster equivalent diameter (d_{cl}) could be found in the author's group [30].

Table 2. Governing equations of gas and particles in the simulation [25].

Continuity Equation of Gas Phase

$$\frac{\partial}{\partial t}\left(\varepsilon_g \rho_g\right) + \nabla \cdot \left(\varepsilon_g \rho_g \vec{u}_g\right) = 0$$

Momentum Equation of Gas Phase

$$\frac{\partial}{\partial t}\left(\varepsilon_g \rho_g \vec{u}_g\right) + \nabla \cdot \left(\varepsilon_g \rho_g \vec{u}_g \vec{u}_g\right) = -\varepsilon_g \nabla p_g - \nabla \cdot \left(\varepsilon_g \tau_g\right) + \varepsilon_g \rho_g g - \vec{F}_D$$

Liouville Equation for Describing the Motion of Particle Phase

$$\frac{\partial f}{\partial t} + \nabla\left(f\vec{u}_p\right) + \nabla_{u_p}\left(fA\right) = 0$$

Particle Acceleration

$$A = D_p\left(\vec{u}_g - \vec{u}_p\right) - \frac{1}{\rho_p}\nabla p + g - \frac{1}{\varepsilon_p \rho_p}\nabla \tau_p$$

Particle Normal Stress Model

$$\tau_p = \frac{P\varepsilon_p^\beta}{\max\left[\left(\varepsilon_{cp} - \varepsilon_p\right), \varepsilon_1\left(1 - \varepsilon_p\right)\right]}$$

Drag Model

$$\vec{F}_D = \beta\left(\vec{u}_g - \vec{u}_p\right)$$

Table 3. Drag force models used for the simulation of downer and riser.

Cluster-Based Drag Model Adopted in Downer [30]

$$\beta = \frac{3}{4}\frac{\varepsilon_g \varepsilon_p |\vec{u}_g - \vec{u}_p|}{d_{cl}}\rho_g C_{dcl}\varepsilon_g^{-2.7}$$

$$C_{dcl} = \frac{24\left(1+0.15\mathrm{Re}_{cl}^{0.678}\right)}{d_{cl}} \quad (\mathrm{Re}_{cl} < 1000)$$

$$C_{dcl} = 0.44 \quad (\mathrm{Re}_{cl} \geq 1000)$$

$$\mathrm{Re}_{cl} = \frac{\varepsilon_g \rho_g |\vec{u}_g - \vec{u}_p| d_{cl}}{\mu_g}$$

EMMS-Based Drag Model Adopted in Riser [28]

$$\beta = \frac{3}{4}\frac{\varepsilon_g \varepsilon_p |\vec{u}_g - \vec{u}_p|}{d_p}\rho_g C_{d0}\varepsilon_g^{-2.7}H_D$$

$$C_{d0} = \frac{24\left(1+0.15\mathrm{Re}_p^{0.678}\right)}{d_p} \quad \left(\mathrm{Re}_p < 1000\right)$$

$$C_{d0} = 0.44 \quad \left(\mathrm{Re}_p \geq 1000\right)$$

$$\mathrm{Re}_p = \frac{\varepsilon_g \rho_g |\vec{u}_g - \vec{u}_p| d_p}{\mu_g}$$

$$H_D = a\left(\mathrm{Re}_p + b\right)^c$$

$$a = \begin{cases} \exp\left(0.5120 + 471.7406\varepsilon_g^{2.5} + 116.8694\frac{\varepsilon_g}{\ln \varepsilon_g}\right) & 0.457 \leq \varepsilon_g < 0.8 \\ \dfrac{1}{\left(0.5690+11201.4430\ln^2 \varepsilon_g - \frac{0.0001868}{\ln \varepsilon_g}\right)} & 0.8 \leq \varepsilon_g < 0.9997 \\ 1 & 0.9997 \leq \varepsilon_g < 1 \end{cases}$$

$$b = \begin{cases} \dfrac{\varepsilon_g}{\left(-0.05570\times\exp\left(-\exp\left(92.9004-209.2822\varepsilon_g\right)\right)\right)}+9.4089 & 0.457 \leq \varepsilon_g < 0.48 \\ -0.8456 \times \exp\left(-\exp\left(141.1489 - 281.1403\varepsilon_g\right)\right)+0.8560 & 0.48 \leq \varepsilon_g < 0.6 \\ -0.001343 \exp\left(\frac{\left(\ln \varepsilon_g + 0.2708\right)^2}{0.01890}\right)+0.06095 & 0.6 \leq \varepsilon_g < 0.98 \\ 0.6141 - 0.5982 \times \exp\left(-361.6032\varepsilon_g^{1177.6292}\right) & 0.98 \leq \varepsilon_g < 0.9997 \end{cases}$$

$$c = \begin{cases} \dfrac{0.5498}{\left(\left(1+\exp\left(23.4547-44.0615\varepsilon_g\right)\right)^{\frac{1}{0.3682}}\right)} & 0.457 \leq \varepsilon_g < 0.622 \\ 0.9387 - 0.3931\varepsilon_g^{63.0517} - 0.4291 \times \exp\left(\varepsilon_g\right) + \frac{0.6075}{\varepsilon_g^{-0.9801}} & 0.622 \leq \varepsilon_g < 0.9997 \\ 0 & 0.9997 \leq \varepsilon_g < 1 \end{cases}$$

2.3. Simulation Set-Up

The simulation was conducted by the commercial software Barracuda® using CPFD approach. The gas and particles in the downer were introduced from the top inlet, while the gas flowed into the riser from the bottom main tube and the particle entered from the side tube near the bottom of the riser. The gas-solids velocity inlet was set on the basis of the experimental superficial gas velocity and the solids circulating flux. The pressure outlets of the gas phase and particle phase were chosen at the bottom of the downer and at the top of the riser, respectively. Normal pressure and temperature were set in the simulation. No-slip wall boundary condition was selected for the gas phase. For the particle phase, the wall boundary condition was described by normal-to-wall retention and tangent-to-wall retention parameters. The grid independency test had been conducted in the previous works of the authors' research group, and found that the simulation results were independent from the mesh size [28,30]. The detailed modeling parameters for simulating the downer and riser are shown in Table 1.

3. Results and Discussion

The accuracy of the CPFD model should be validated before its further usage in analyzing the hydrodynamics in the CFB riser and downer. In the previous works of the authors' research group, the model has been validated, which shows that the current CPFD model can be accurately adopted to predict the hydrodynamics in both the CFB riser and downer [28,30].

Before the simulation results were used for analysis, the predicted flow structure should be confirmed to have achieved statistically stabilized state. The time evolutions of particle inventory inside the downer and riser, as shown in Figure 2, were used to determine whether the predicted flow structure had reached stabilized state. It is obvious from the figure that the particle inventory

inside the downer increased dramatically in 1 s from the beginning and stayed nearly unchanged after 1 s, indicating that the predicted gas-solids flow in downer quickly reached stabilized state in 1 s. In contrast, the particle inventory inside the riser increased slowly in 10 s from the beginning and changed slightly after 10 s, indicating that the predicted flow structure in riser experienced a relatively slow flow development and reached statistically stabilized state after 10 s. It should be mentioned that the fluctuation of particle inventory after 10 s is mainly caused by the non-uniform particle flow and back-mixing behaviors inside the riser. This is common phenomena in such a complex gas-solids system as riser. In the present work, the simulation results were statistically averaged after 10 s for both downer and riser.
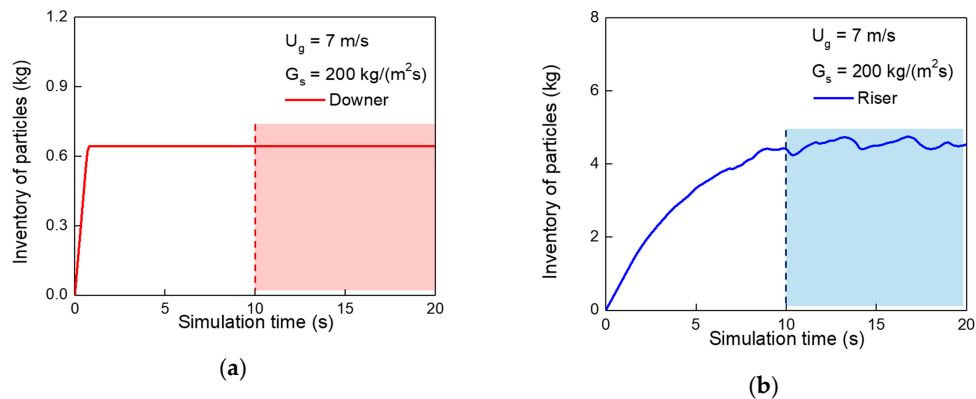
Figure 2. Time evolution of the particle inventory inside the circulating fluidized bed (CFB) downer and riser. (**a**) Downer; (**b**) riser.

The axial distribution of the time-averaged pressure difference inside the downer and riser were shown in Figure 3. The pressure difference between the bed and the inlet is defined as (P_0-P), where P_0 is the time-averaged pressure at different heights and P is the operating pressure at the inlet (101,300 Pa) as shown in Table 1. In the downer, the pressure decreased significantly from the inlet to the middle part and then increased to the outlet. This trend was consistent with the experimental study by Zhang et al. [9]. In the riser, the pressure decreased from the inlet to the outlet, which was in accordance with the study by Wang et al. [37]. The difference of pressure from the inlet to the outlet was the driving force for the upward gas-solids flow.
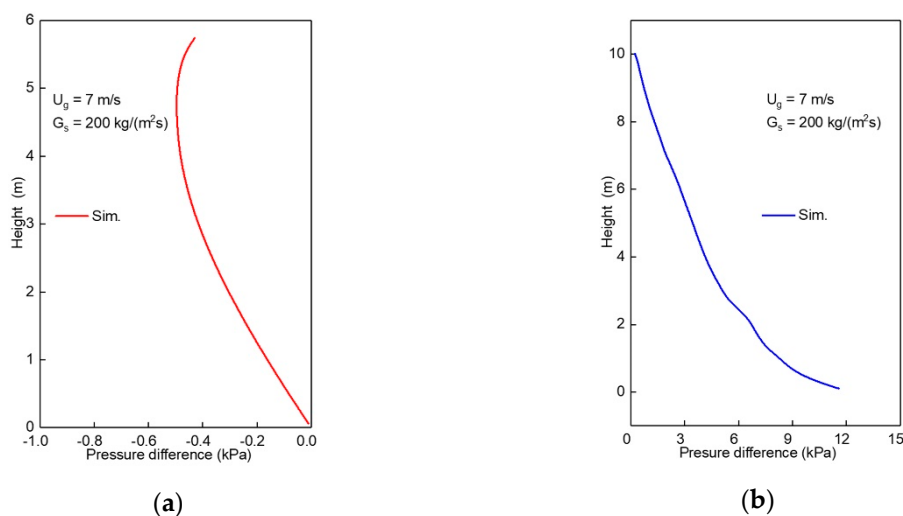

Figure 3. Predictions of axial distribution of time averaged pressure difference inside the downer and riser. (**a**) Downer; (**b**) riser.

3.1. Solids Holdup

As a method based on the Eulerian–Lagrangian framework, the CPFD approach can track the motion of individual particles and analyze the characteristics of particles in detail. As demonstrated in the previous works [28,30], the gas-solids flow pattern of downer and riser can be out of the influential region of the inlet structure at the axial position of 5 m from the inlet. Therefore, the following discussions would focus on the simulation results at this height of 5 m. The instantaneous solids holdup, which is the solids holdup at a specified time, was compared in the downer and riser. The predicted overall and local distributions of the cross-sectional solids holdup in the downer and riser are shown in Figure 4. In order to better demonstrate the simulation results, the particle size in the downer and riser were scaled up by six times and 12 times respectively. Different colors indicated different particle concentrations. From the axial distribution of solids holdup in the downer, it can be seen that particles tended to gather near the inlet region. According to the equation of calculating the solids holdup ($\varepsilon_p = \frac{G_s}{\rho_p u_p}$), when the solids mass flux (G_s) is fixed, the lower the particle velocity, the higher the solids holdup. Thus, higher solids holdup near the inlet region may cause the physical phenomenon that is particle gathering near the inlet. As the particles flowed downward, particle concentration decreased to a nearly constant value. In the radial direction, particle concentration distributed uniformly. In the CFB riser, the CPFD approach predicted "bottom dense and top dilute" flow structure in the axial direction, which was also observed by previous experimental study [38]. In the radial direction, particles were concentrated and aggregated together to form clusters both in the center and near the wall. More clusters were predicted near the wall than in the center, and the dispersed particle phase tended to be present in the center, resulting in diluted particle concentration in the central area and higher particle concentration near the wall. At the same operating condition, the solids flow was more uniform in the downer compared to the riser along the axial direction. Although the solids holdup in the downer was much lower than that in the riser under the same operating condition [28,30], the clustering phenomenon with a small amount of particles aggregating together can still be observed from the Figure 4a. The size of clusters in the downer was much smaller than that in riser.
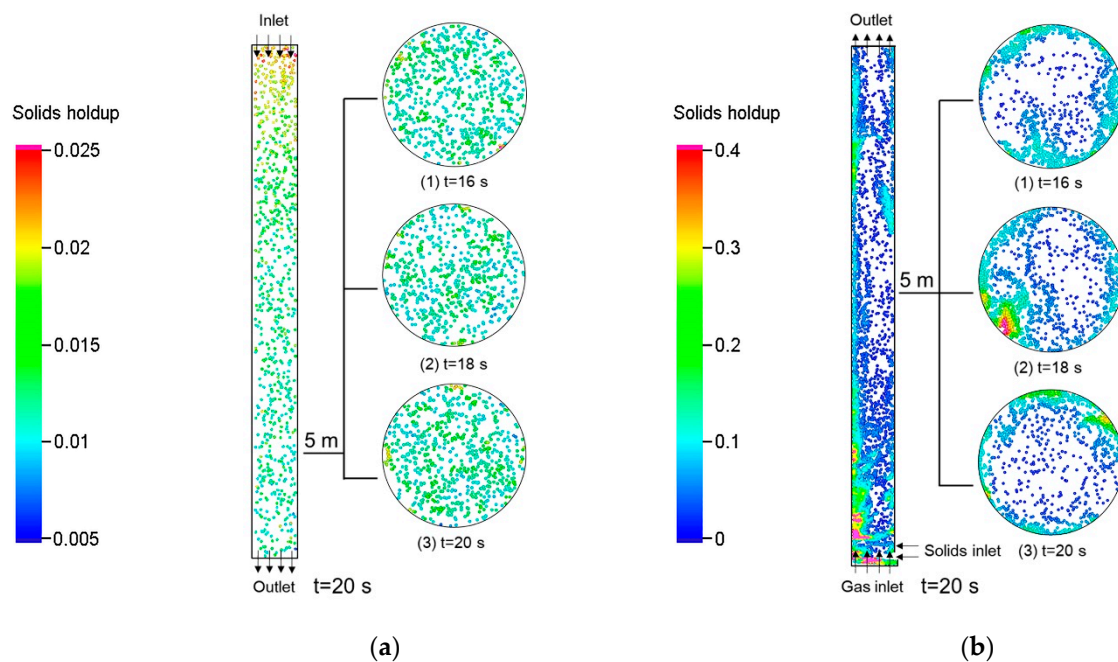

Figure 4. Instantaneous distributions of solids holdup inside the downer and riser at different times (axial distribution at 20 s and radial distribution at 16, 18, and 20 s, respectively) for the (**a**) downer; and (**b**) riser.

To further reveal the difference with respect to the cluster behaviors and the micro flow structure in the downer and riser, the local solids holdup at the simulation time of 18 s at the height of 5 m were analyzed statistically to obtain the probability density distribution (PDD) of instantaneous solids holdup in the downer and riser, as shown in Figure 5. The figure displayed unimodal distribution and bimodal distribution in downer and riser, respectively. In the downer, only one peak was predicted with the solids holdup of most particles less than 0.02, as shown in Figure 5a, and this was consistent with the reports of Zhang et al. [39]. This type of single peak revealed that the particles in the downer were mostly in the form of a dispersed particle phase. In the riser, except for the dispersed particle phase with low solids holdup less than 0.02, there still existed another peak with solids holdup higher than 0.1, which indicated cluster phase. This predicted phenomenon was similar to the experimental results reported by Lin et al. [40]. It can be concluded from the PDD of the riser that particles with a solids holdup over 0.1 occupied a probability of over 25%, which indicated that the cluster phase played a critical role in determining the solids holdup. The PDD of the downer and riser both showed a peak at the solids holdup less than 0.02, which indicated that the dispersed particle phase with low particle concentrations existed in both the downer and riser. Different forms of solids holdup PDD in the downer and riser indicated that the clustering phenomena in the downer was different from that in riser.
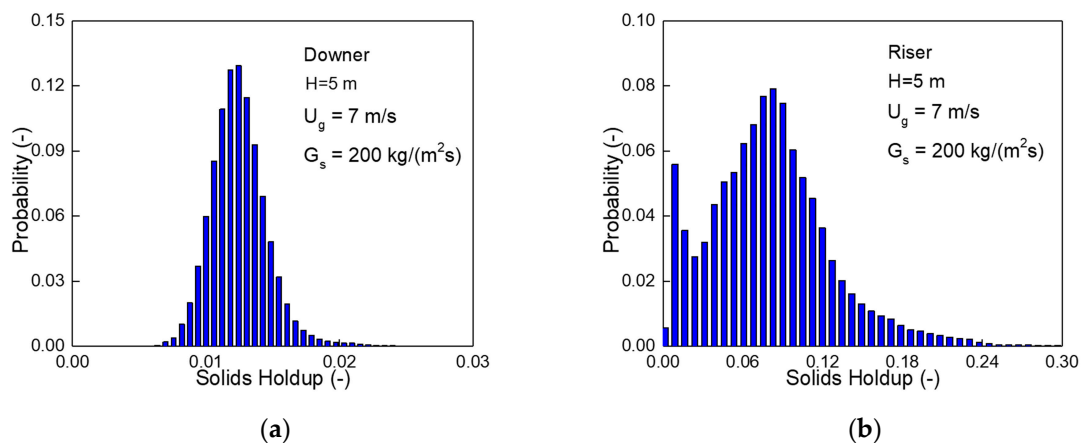

| (a) | (b) |

Figure 5. Probability density distribution of instantaneous solids holdup in downer and riser (H = 5 m). (**a**) Downer; (**b**) riser.

For further analyzing the solids holdup non-uniformity in radial direction, the radial non-uniformity index (RNI) firstly proposed by Zhu and Manyele [41] was used to quantitatively compare the difference of radial distribution of solids holdup between downer and riser. The definition of RNI(ε_p) was

$$\text{RNI}(\varepsilon_p) = \frac{\sigma(\varepsilon_p)}{\sigma(\varepsilon_p)_{\max}} = \frac{\sigma(\varepsilon_p)}{\sqrt{\bar{\varepsilon}_p(\varepsilon_{p,mf} - \bar{\varepsilon}_p)}} \tag{1}$$

where $\sigma(\varepsilon_p)$ is the standard deviation of the radial cross-sectional solids holdup, $\sigma(\varepsilon_p)_{\max}$ is the maximum possible standard deviation of solids holdup, $\varepsilon_{p,mf}$ is the highest possible solids holdup which is the packing limit depending on the particle properties and in this study this value is 0.6 as shown in Table 1, and $\bar{\varepsilon}_p$ is the average solids holdup obtained by sampling the particles at the local cross-sectional area. The value of RNI(ε_p) varies between 0 and 1. If the particles were completely distributed uniformly in the radial direction, indicating that there was almost no deviation of solids holdup at the radial position, the RNI(ε_p) value would be 0. On the contrary, if particles gathered with maximum solids holdup (for example near the wall) of $\varepsilon_{p,mf}$, the value of RNI(ε_p) would be 1.

The time-averaged RNI(ε_p) in the downer and riser at the same operating condition was obtained from the transient data from 10 s to 20 s. At a height of 3, 4, and 5 m, the time-averaged RNI in

the downer is 0.0225, 0.0224, and 0.0213, respectively; and in the riser is 0.3871, 0.3591, and 0.3528, respectively. In the downer, the RNI(ε_p) was about 0.02, indicating that the solids flow in the downer was almost in completely uniform state. Compared to the downer, the RNI(ε_p) in the riser was about 0.3–0.4, which was over 10 times higher than that in the downer. These results were similar to the experimental research of Wang et al. [16].

To further analyze the difference of cluster characteristics observed in Figure 4 between the downer and riser, the predicted time evolutions of solids holdup in the center and near the wall at three different radial heights were presented, as shown in Figures 6 and 7. In the riser, most particles were in the form of a dispersed particle phase with a low concentration and smaller fluctuation in the central area. However, the cluster behavior with the peak value of solids holdup can still be captured in the center in this figure. The peak was narrow indicating that the duration of the cluster was short in the center. In the near wall region of the riser, the cluster peak was wider, indicating the duration of the cluster was longer than that in the central region. These results were consistent with the cluster characteristic reported by Zhang et al. [23]. Compared to the riser, the higher fluctuation frequency of solids holdup in both the central and near wall region of the downer indicated a faster rate of cluster formation and dissolution. The higher fluctuation frequency in the downer also indicated that larger clusters were more difficult to be formed in the downer than that in the riser.
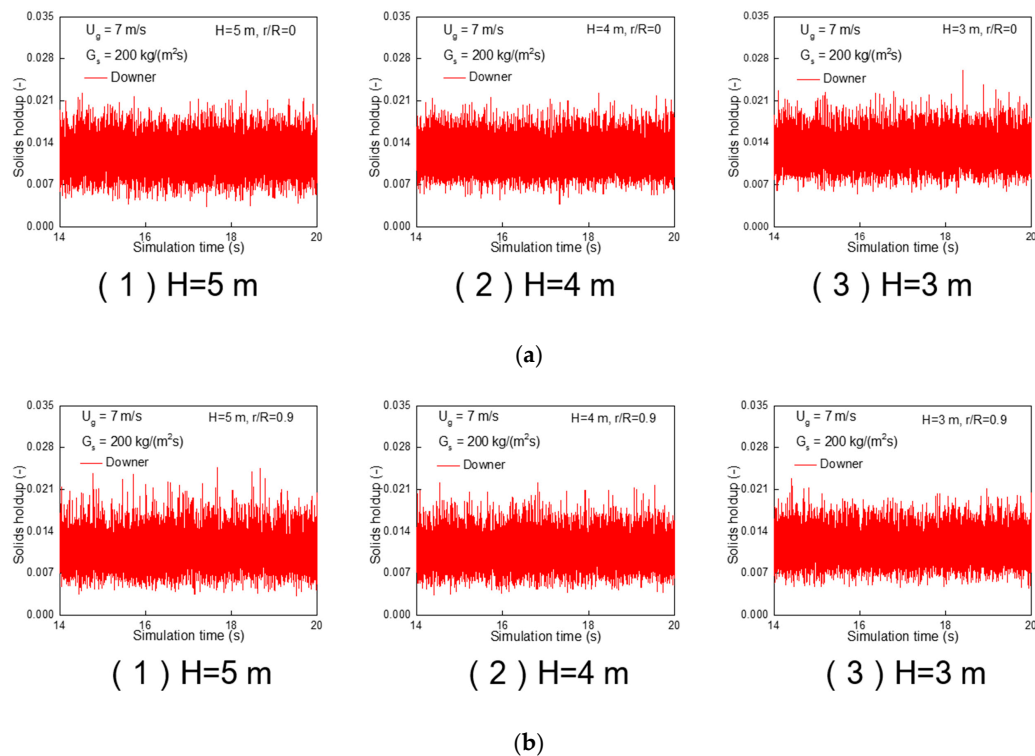

Figure 6. Predicted time evolution of local solids holdup at center and near the wall in downer (H = 5 m, 4 m, 3 m). (**a**) Center; (**b**) wall.

The power spectral density is a type of method used to analyze the random signal. The solids holdup signals in Figures 6 and 7 were analyzed by fast Fourier transform (FFT) to obtain the power spectral density of different heights in downer and riser shown in Figures 8 and 9. The power spectral density was used to characterize the fluctuation intensity of signal under different frequencies. It was obvious that the power spectral density was much higher in riser than in downer under low frequency, which indicates that more clusters were broken into dispersed particles in riser compared with downer. On the contrary, the power spectral density in downer was higher than that in riser under high frequency which represents that the cluster in downer was more unstable.
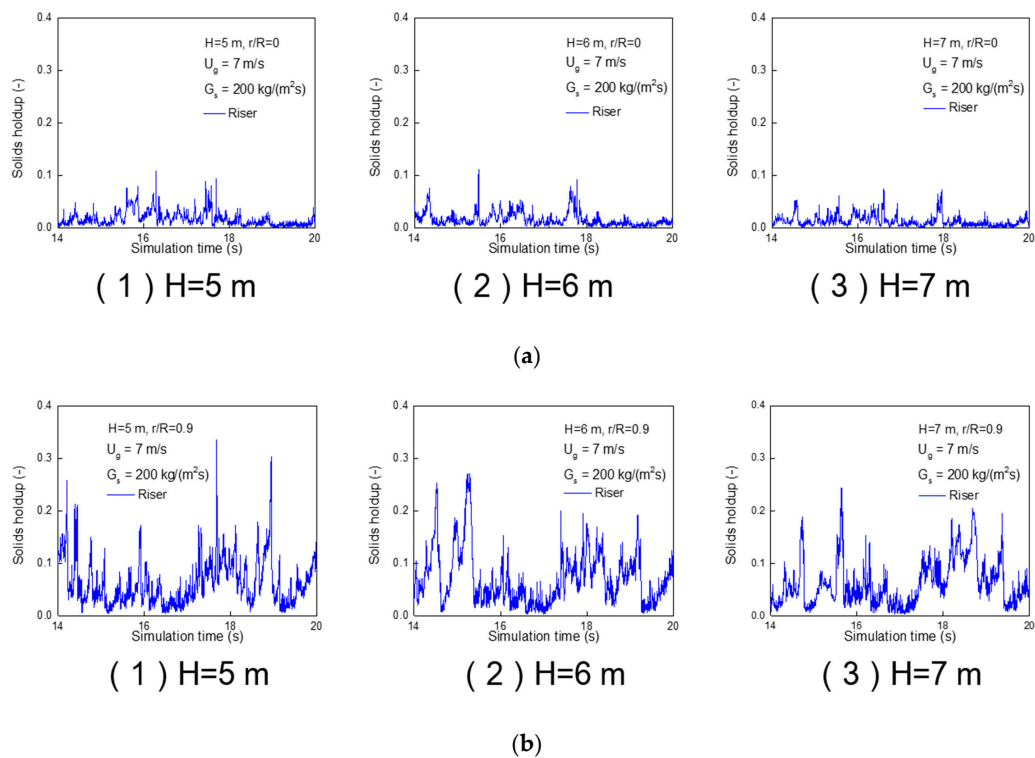
Figure 7. Predicted time evolution of local solids holdup at center and near the wall in riser (H = 5 m, 6 m, 7 m). (**a**) Center; (**b**) wall.
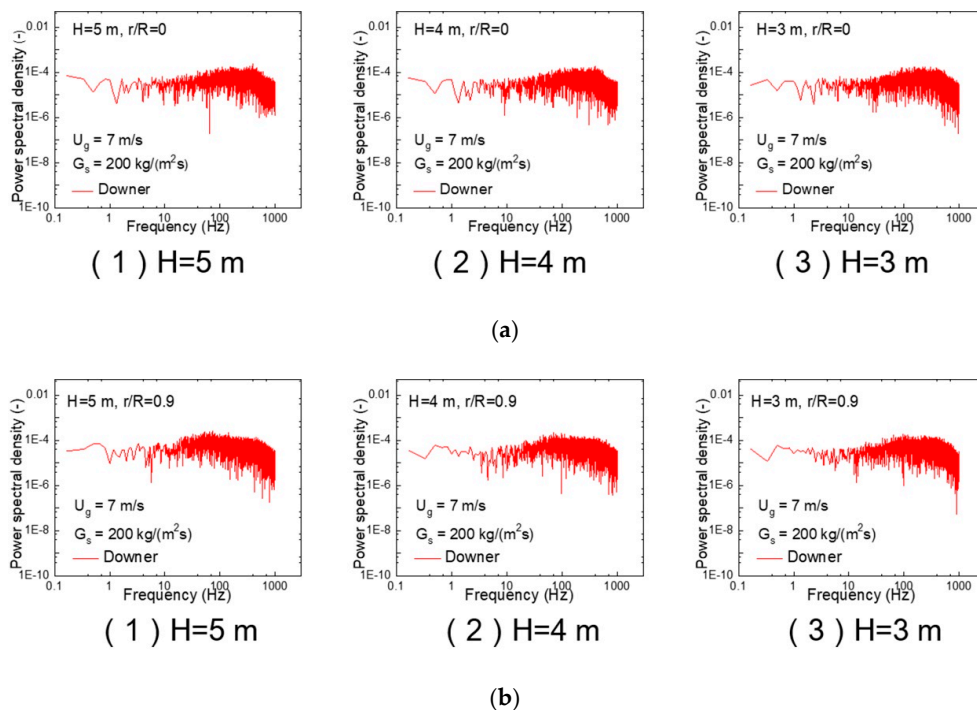

Figure 8. Power spectral density analysis of solids holdup signals in downer under different heights. (**a**) Center; (**b**) wall.
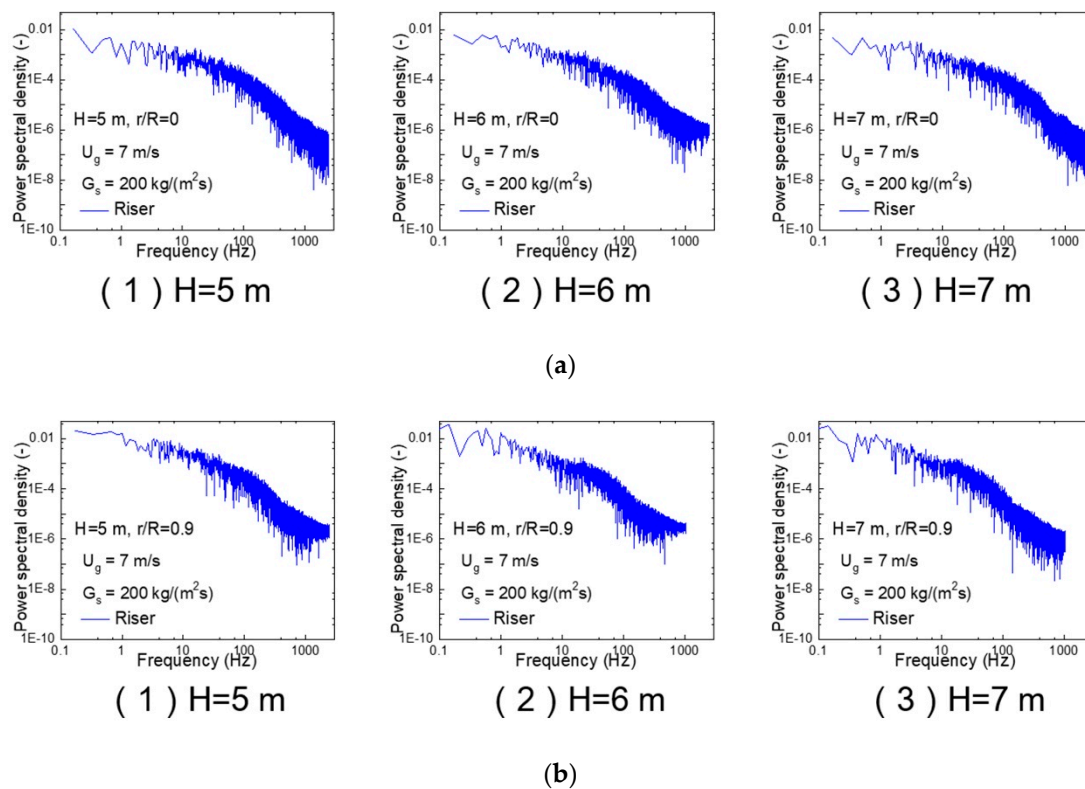
Figure 9. Power spectral density analysis of solids holdup signals in riser under different heights. (**a**) Center; (**b**) wall.

Figure 10 shows the instantaneous distribution of cluster at different simulation times from the height 5 m to 5.5 m. In order to better display the cluster behavior in downer, the particle size was enlarged 3 times. The cluster size was smaller and the clusters distributed in the whole downer compared to the riser. Clusters in downer showed stick shape, and it was similar to the cluster shape reported by Lu et al. [42] employing the micro-video action shot, and by Gomez and Molina [43] using the DEM. In the riser, the cluster with much higher particle concentrations tended to be gathered near the wall, as also demonstrated in Figure 4b. The cluster near the wall in riser exhibited various shapes, such as a vertical strand shape and ellipsoid shape, which was in accordance with the experimental phenomenon observed by Shaffer et al. [44] using high-speed digital image technology. In addition, a typical "V" shape cluster was also captured as shown in Figure 10b, and it was similar to the experimental results visualized by Xu and Zhu [45] using high-speed digital image system, and by Zhang et al. [23] employing the DEM and by Liu and Lu [46] with direct simulation Monte Carlo (DSMC) method respectively.
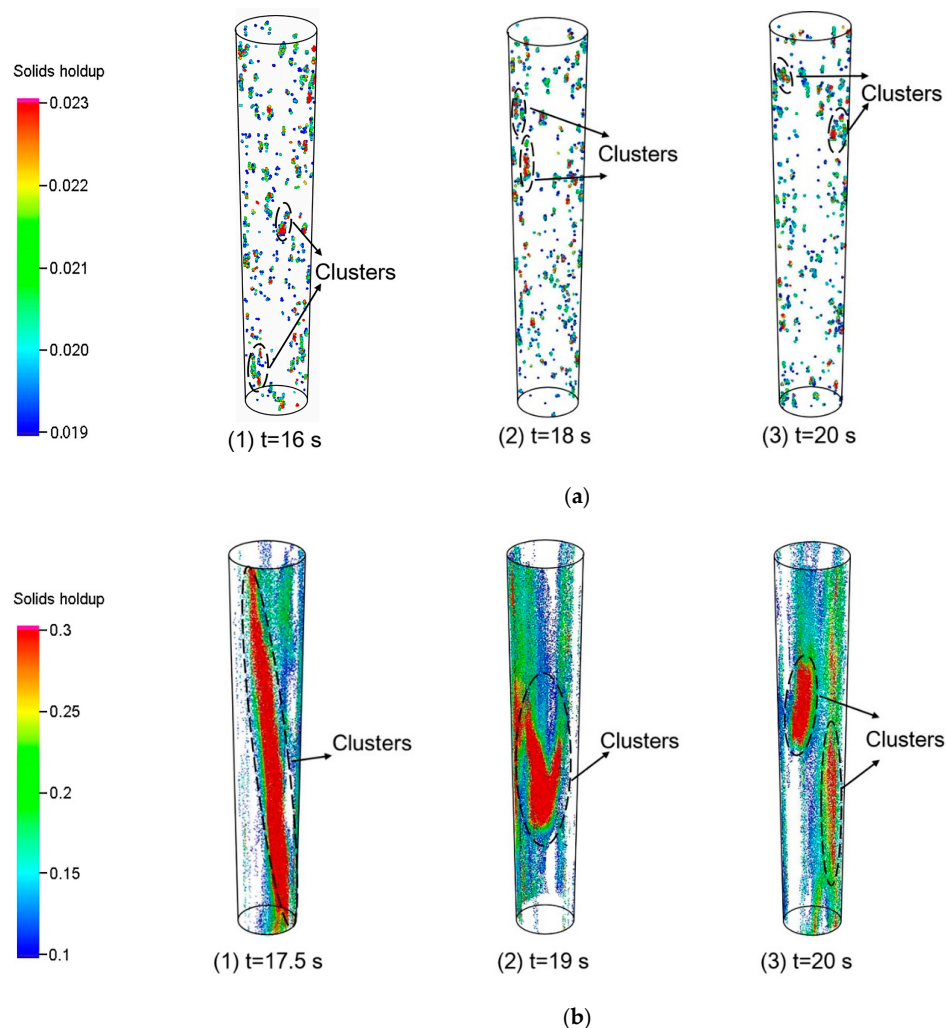
Figure 10. Schematic of clusters in downer and riser at various transient simulation times (H = 5~5.5 m). (**a**) Downer; (**b**) riser.

3.2. Solids Velocity

The instantaneous distributions of solids vertical velocity in the downer and riser, including the axial distribution of the whole bed as well as the radial distribution at the height of 5 m were shown in Figure 11. In the downer, the blue color represents the downward particles with lower velocity and the red color represented the faster downward particles. In the riser, the blue represents the particles moving downwards while the green and red represents the upward particles. From Figure 11a, the solids vertical velocity was lower near the inlet of the downer, and it was increased dramatically within a very short distance from the inlet due to the co-function of gravity and drag force. Then the solids vertical velocity was almost stable at the middle part of the downer due to the balance of gravity and drag force. In the radial direction of downer, the distribution of solids vertical velocity at the height of 5 m was relatively uniform except near the wall. The solids vertical velocity near the wall was slightly lower than that in the center due to the wall effects.

The solids vertical velocity was more non-uniform in both the axial and radial direction of the riser than that of downer. In the axial direction of the riser, the solids vertical velocity increased and then decreased at the co-function of gravity and drag force. In the radial direction of the riser, particles tended to flow upward in the center and downward near the wall. Such downward flow can cause solids back-mixing, which was mainly due to the dynamic process that clusters formed and broke near the wall region.
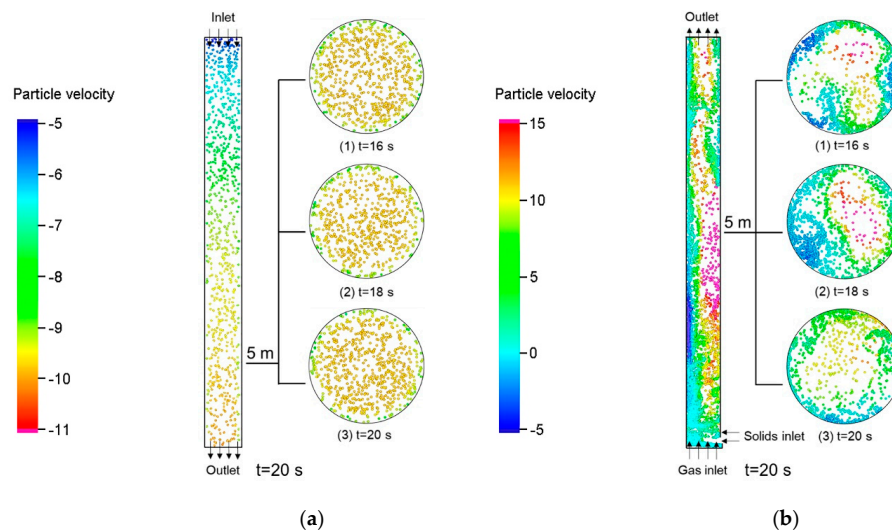
Figure 11. Instantaneous distributions of solids vertical velocity at different time (axial distribution at 20 s and radial distribution at 16, 18, and 20 s, respectively) for the (**a**) downer; and (**b**) riser.

Similar to the sampling process to obtain the PDD of solids holdup shown in Figure 5, the PDD of the solids vertical velocity were shown in Figure 12. In the downer, a single peak with high downward velocity was predicted, indicating that most particles (with a probability over 60%) in the downer existed in the form of dispersed particle phase. In the riser, particles with negative velocity showed a probability of over 40%, indicating that a large portion of particles were in the form of a cluster. Dispersed particle phase with high velocity (more than 10 m/s) was also captured in the riser. Clusters with a larger size can be formed in the riser than that in the downer. Large clusters have higher gravity, and tend to flow downward near the wall.
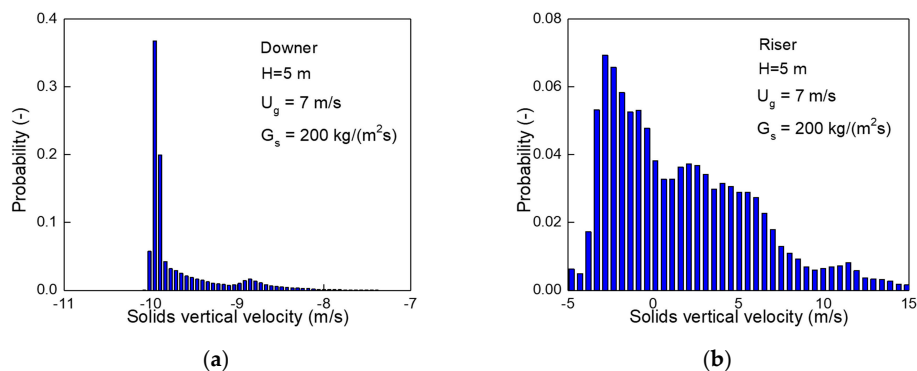

Figure 12. Probability density distribution of instantaneous solids vertical velocity in downer and riser (H = 5 m). (**a**) Downer; (**b**) riser.

The time evolution of the local instantaneous solids vertical velocity inside the downer and riser at three different radial heights were statistically sampled, as shown in Figures 13 and 14. In the downer, the overall fluctuation of particle velocity was much smaller, indicating that the particles in the downer were uniformly distributed as dispersed particle phases or small clusters. The fluctuation of solids velocity in the near wall area was higher than that in the center, which indicates that the frequency of cluster formation and dissolution near the wall was higher than that in the central area. Larger fluctuations, which are mainly due to the dynamic formation and dissolution of clusters, of solids vertical velocity was present in both the center and the near wall region in the riser, showing that clusters existed in both the central area and the near wall region.

Overall, the solids vertical velocity in the riser fluctuated more greatly, which further explains that the gas-solids flow in downer was more uniform than that in riser.
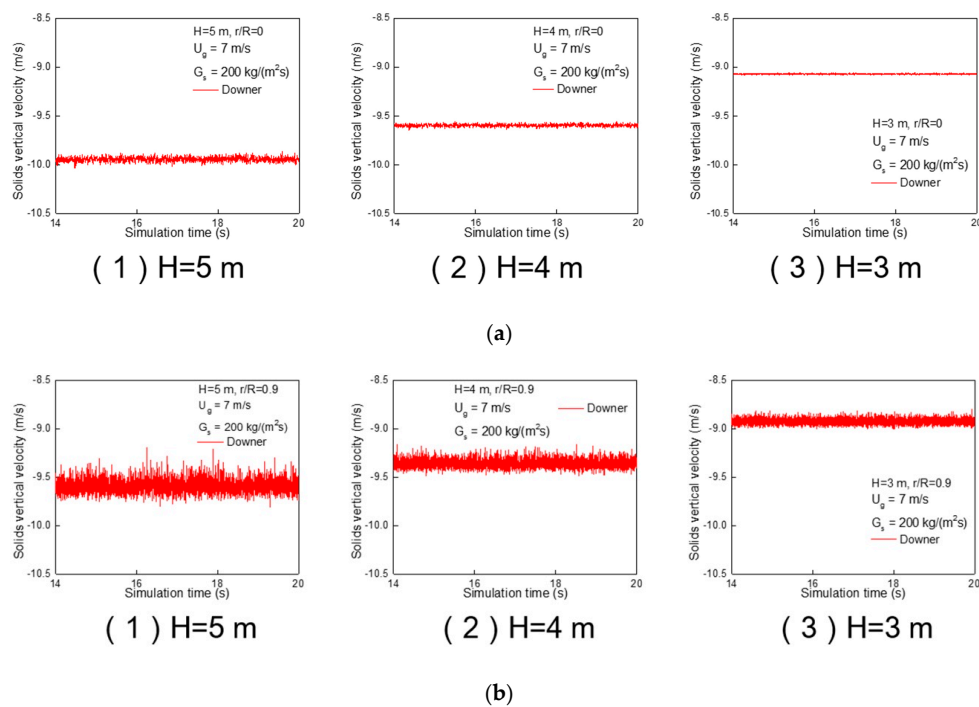
Figure 13. Predicted time evolution of local instantaneous solids vertical velocity at the center and near the wall in downer (H = 5, 4, and 3 m). (**a**) Center; (**b**) wall.
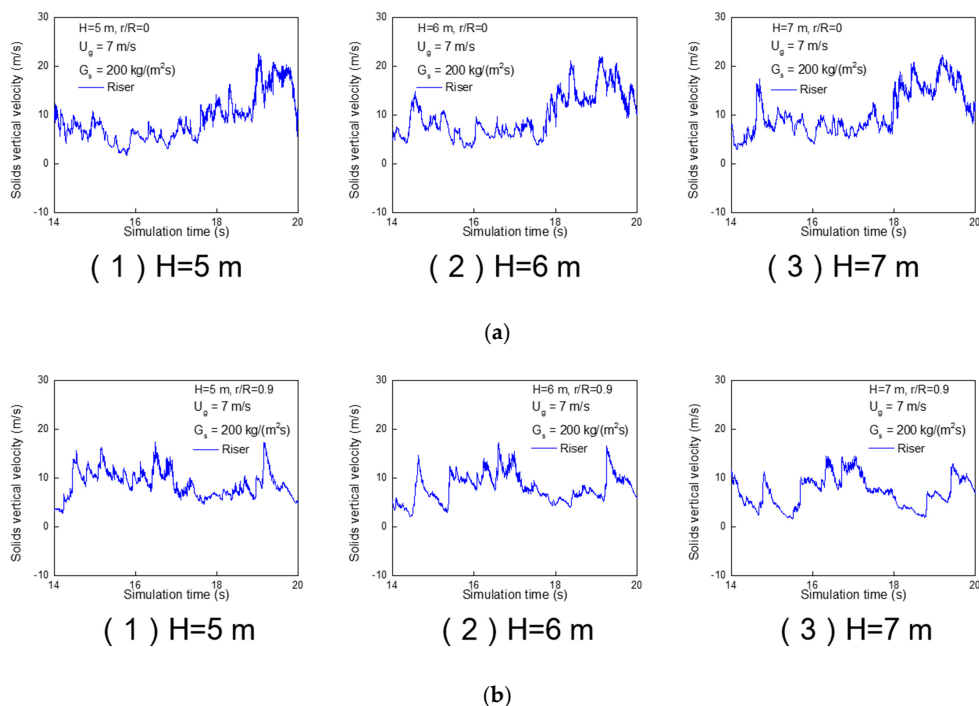

Figure 14. Predicted time evolution of local instantaneous solids vertical velocity at center and near the wall in riser (H = 5, 6, and 7 m). (**a**) Center; (**b**) wall.

Next, the difference of local instantaneous solids radial velocity between the downer and riser was revealed to provide detailed information about the radial uniformity characteristics, which is a crucial factor to affect the radial solids holdup distribution. Time evolutions of solids radial velocity are shown in Figures 15 and 16. In the downer, the overall fluctuation of the solids radial velocity was much weaker compared with riser. Meanwhile, the flow development in the downer would intensify

the fluctuation since more clusters formed and dissolved with the development of flow. In the riser, a much higher fluctuation was found in the central area than that in the near wall region, which was mainly because the clusters with large volume forming in the near wall region was stable as observed in Figures 7 and 10.
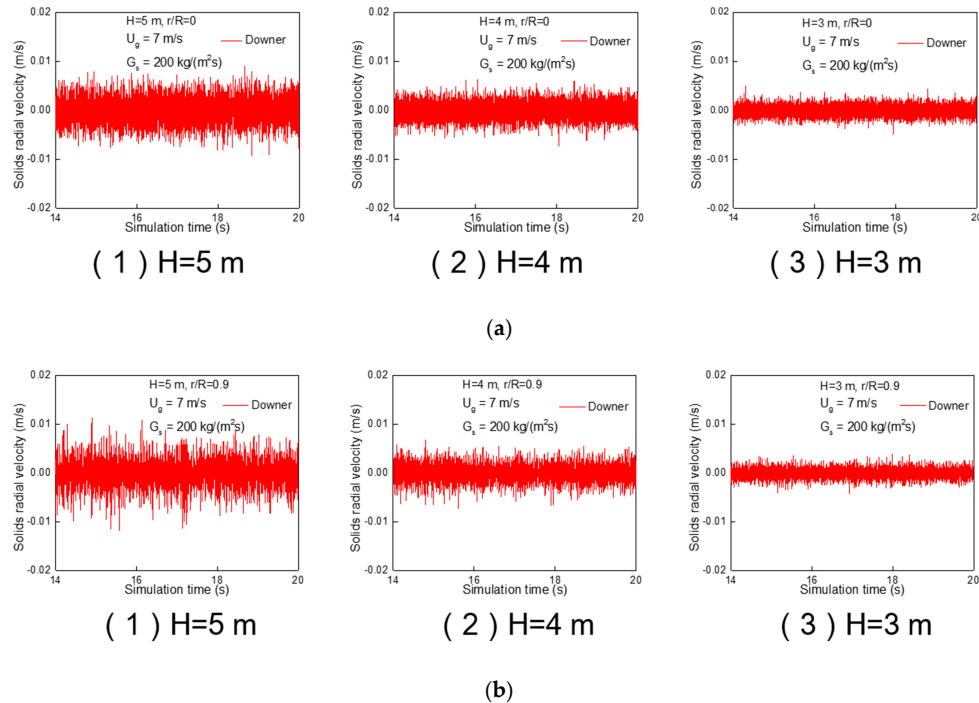

Figure 15. Predicted time evolution of local instantaneous solids radial velocity at center and near the wall in downer (H = 5 m, 4 m, 3 m). (**a**) Center; (**b**) wall.
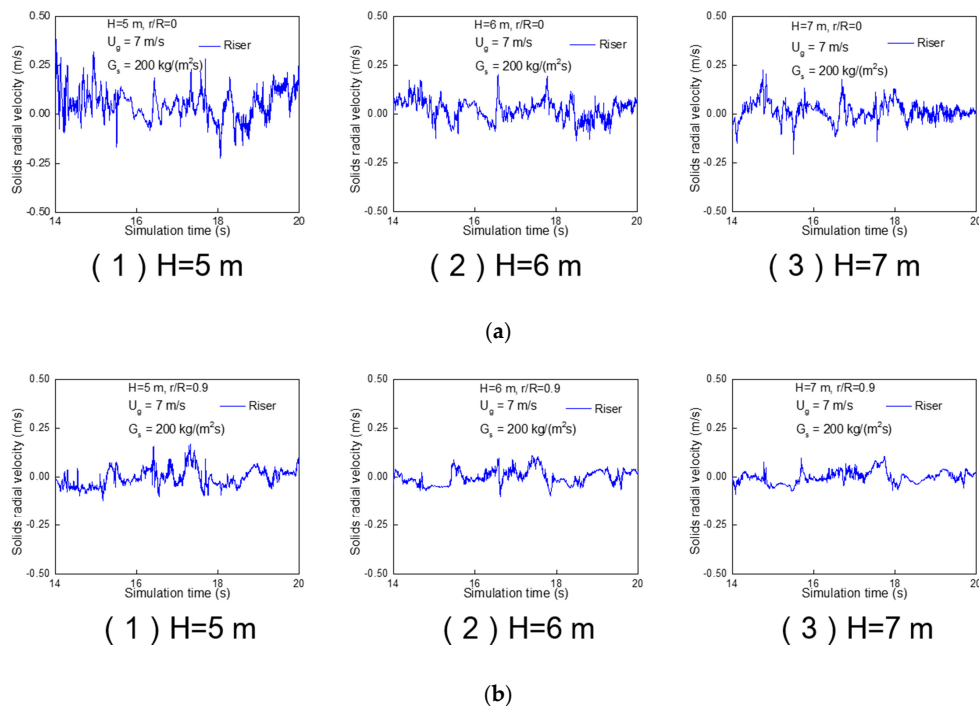

Figure 16. Predicted time evolution of local instantaneous solids radial velocity at center and near the wall in riser (H = 5, 6, and 7 m). (**a**) Center; (**b**) wall.

3.3. Solids Residence Time

In chemical reaction engineering, the conversion rate and selectivity of desired products in the industrial-scale CFB are closely associated with the solids mixing behavior. The residence time distribution (RTD) of the particles is commonly used to reveal the axial solids mixing behavior inside the riser and downer. Particle tracer technology was usually adopted to study the particle RTD in the CFB system in previous experimental studies [47–50]. However, the particle tracing process is complicated and it will interfere with the main particle stream inside the bed. Therefore, the reliability of the experimental results may be limited. The CPFD approach is able to obtain the residence time of each individual particle by directly tracking the motion of the particles inside the CFB system. In the CPFD simulation, the overall particle RTD of the whole CFB system can be obtained by statistical analysis of the particles at the outlet, while the local particle RTD can be obtained by statistical analysis of the particles at the cross-section of a specific height.

The particle RTD in the axial direction and in the radial direction at a height of 5 m were shown in Figures 17 and 18. Blue color showed shorter residence time and red color represented longer residence time. In downer, the particle residence time increased evenly from the top inlet to the bottom outlet. In contrast, particles with both shorter and longer residence time were presented in the whole riser. Some particles with blue color (residence time less than 2 s) can be predicted at the top of the riser, indicating that these particles scarcely underwent back-mixing and flow through the riser quickly. Some particles colored by red (residence time more than 10 s) can still be predicted at the bottom of the riser. This comparison indicates that the particle can flow through the downer with uniform velocity and less back-mixing while severe back-mixing existed in the riser. In the radial direction of the downer, the particle residence time distributed uniformly except for slightly longer residence time near the wall because of the wall friction. In contrast, in the radial direction of the riser, particle residence time ranges from 1 s to 12 s, again indicating severe particle back-mixing. In addition, shorter residence time particles tended to be present in the center while longer residence time particles tended to be present near the wall of the riser, which is mainly because the larger cluster flow downwards in the near wall region.
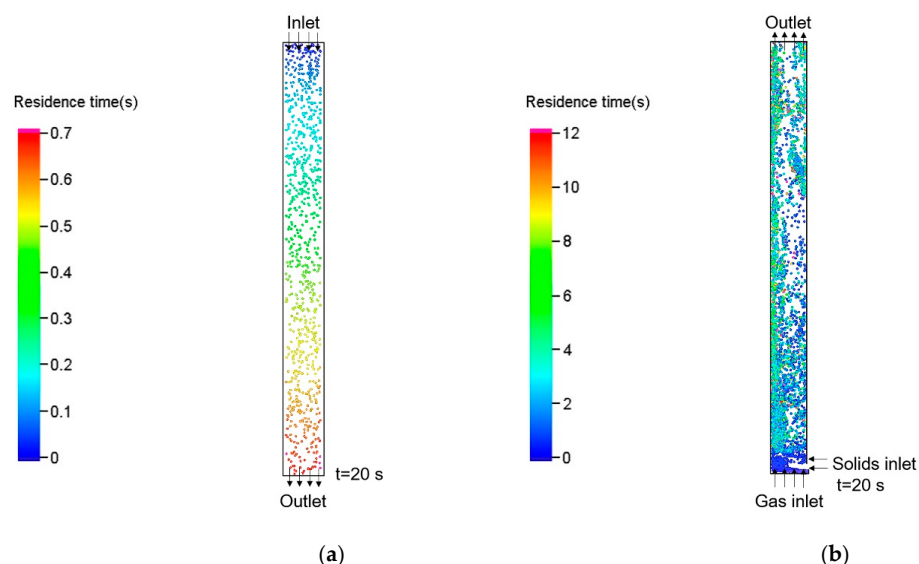

Figure 17. Axial distributions of solids residence time inside downer and riser. (**a**) Downer; (**b**) riser.

In order to further reveal the difference of solids back-mixing degree between the downer and riser, the predicted cumulative distribution of solids RTD (*F(θ)* curve) at the outlet of downer and riser are compared in Figure 19. The slope of *F(θ)* curve is commonly used to reveal the degree of solids back-mixing. Smaller slope represents more intense back-mixing.
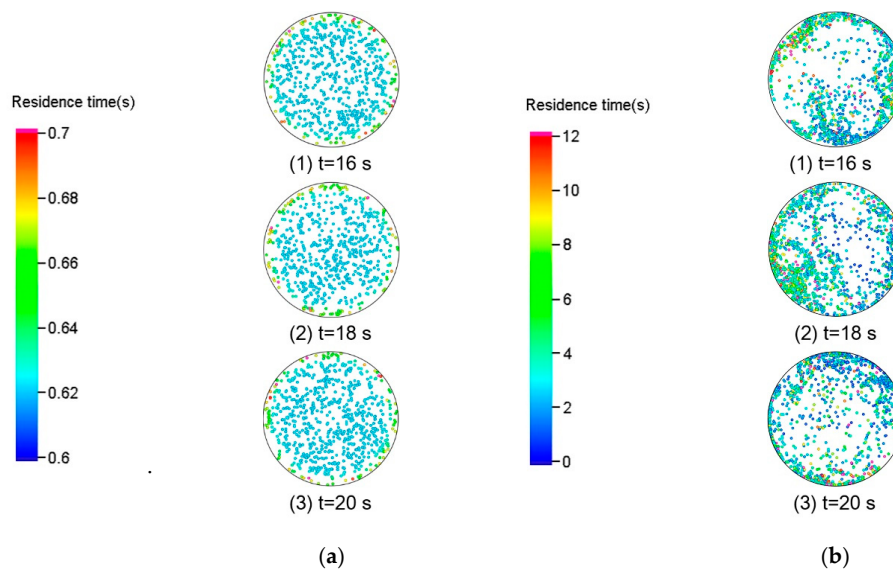
Figure 18. Radial distributions of solids residence time inside downer and riser. (**a**) Downer; (**b**) riser. (H = 5 m).

From this figure, it can be seen that the *F(θ)* curve was much steeper for the downer than for the riser. The *F(θ)* curve of the downer was almost vertical, indicating that particles can flow through the downer uniformly with limited back-mixing. The almost vertical *F(θ)* curve of the downer shows that particle flow approached to the ideal plug flow, which was consistent with the experimental results of Huang et al. [51]. In contrast, the slope of the *F(θ)* curve of riser was smaller, indicating that severe solids back-mixing happened in the riser.
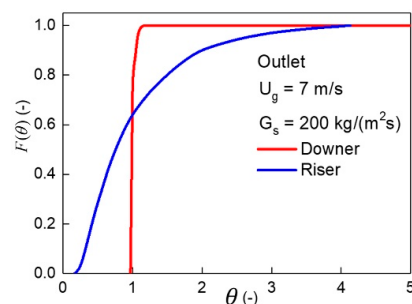

Figure 19. Cumulative distribution of dimensionless solids residence time distribution (RTD) at the outlet of downer and riser.

3.4. Solids Dispersion Coefficient

The solids dispersion coefficient is used to deeply study the solids transportation mechanism as well as solids mixing quality in CFB system. Meanwhile, the solids mixing quality is closely associated with gas-solids contact efficiency and interphase heat transfer and mass transfer performance [52]. Thus, better understanding about the distribution of the solids dispersion coefficient inside the downer and riser is conductive to obtain an optimized and improved performance of the CFB system.

The calculation of solids dispersion coefficient is commonly by macro approach and micro approach [53]. In this study, the latter method was used because CPFD approach can track the trajectory of particles. Additionally, the solids dispersion coefficient of the pilot-scale CFB downer and riser with

Geldart A particles was firstly obtained by the Eulerian–Lagrangian approach. For each individual particle, its solids dispersion coefficient can be expressed as:

$$D_i = \frac{(\Delta r_i)^2}{2\Delta t} \tag{2}$$

where Δr_i is the displacement of particle i at the time interval Δt. The solids dispersion coefficient of each individual particle during a specified time interval could be obtained by the above formula. The statistical analysis focused on the particles in the local area of the CFB system is necessary due to the random solids motion characteristics inside the CFB system. Particles in the local area are sampled and then the solids dispersion coefficient of the local area is obtained by summing and averaging the solids dispersion coefficient of each individual particle, formulated as:

$$D = \frac{1}{n}\sum_{i=1}^{n} \frac{(\Delta r_i)^2}{2\Delta t} = \frac{1}{2 \times \Delta t \times n}\sum_{i=1}^{n} (\Delta r_i)^2 \tag{3}$$

In this study the axial solids dispersion coefficient was obtained by tracking the axial motion of each individual particle and the formula below was used:

$$D_{axial} = \frac{1}{n}\sum_{i=1}^{n} \frac{(\Delta r_{axial})_i^2}{2\Delta t} = \frac{1}{2 \times \Delta t \times n}\sum_{i=1}^{n} (\Delta r_{axial})_i^2 \tag{4}$$

Figures 20 and 21 show the time-evolutions of axial solids dispersion coefficient in downer and riser. It is noted that the axial solids dispersion coefficient fluctuated over time in both downer and riser due to the random motion of gas-solids two phase flow. The overall fluctuation of axial solids dispersion coefficient in the downer was much weaker indicating that the solids transportation ability was stable during the continuous operation of downer. Compared to the downer, the fluctuation of axial solids dispersion coefficient was much stronger which was mainly caused by the formation and dissolution of large volume cluster.
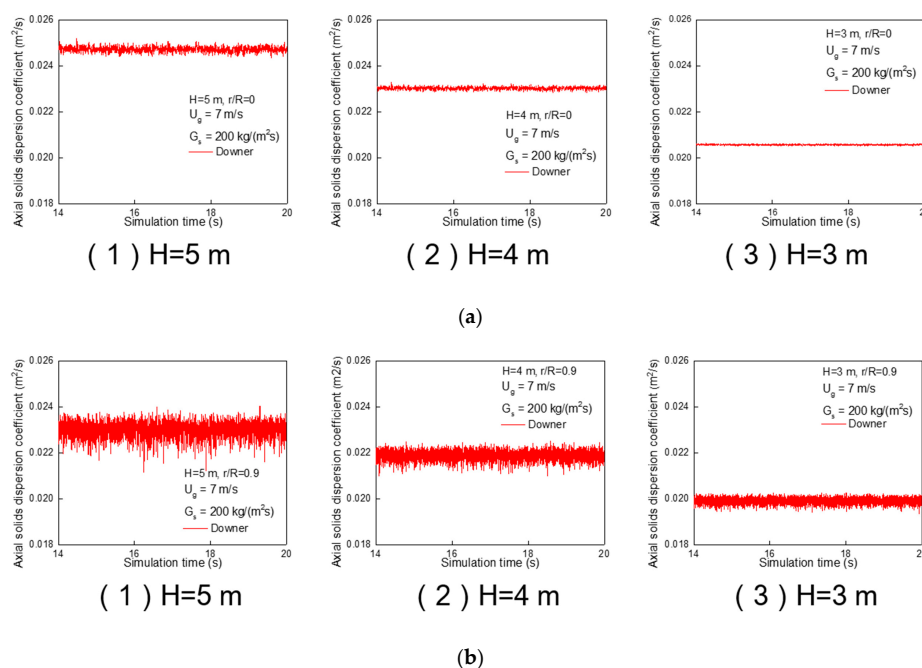

Figure 20. Predicted time evolution of axial solids dispersion coefficient inside downer (H = 3, 4, and 5 m). (**a**) Center; (**b**) wall.
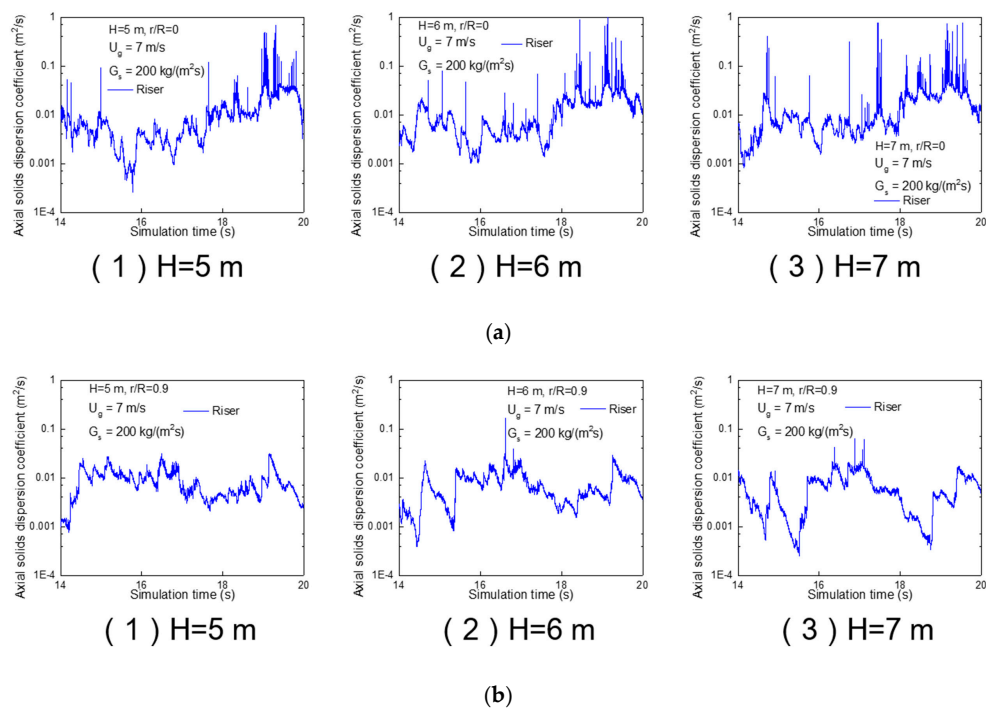
Figure 21. Predicted time evolution of axial solids dispersion coefficient inside riser (H = 5, 6, and 7 m). (**a**) Center; (**b**) wall.

After that, the instantaneous axial solids dispersion coefficients from 14 s to 20 s were statistically averaged to obtain the time-averaged axial solids dispersion coefficients. Then, the time-averaged axial solids dispersion coefficients in the center and near wall region between the downer and riser were compared with those in previously reported experiment [54–58] and simulation results [59], that is shown in Figure 22. The computation results in this study was in the range of the previous experiment and simulation research. The axial solids dispersion coefficient in the downer was higher than that in the riser, which indicated that the solids transportation ability in the downer was higher when the operating conditions were the same. In the riser, the large volume cluster formation near the wall caused a 67% decrease of axial solids dispersion coefficient compared with the central area.
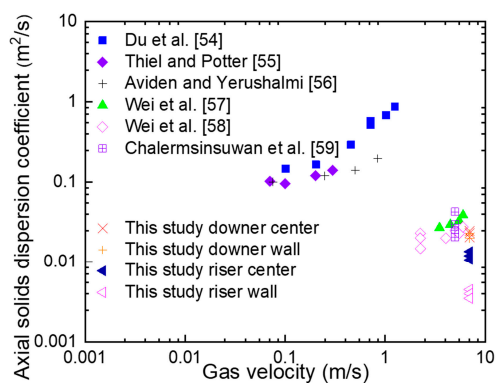

Figure 22. Comparisons of computed time-averaged axial solids dispersion coefficient inside the downer and riser with those previously reported experiment and simulation results.

3.5. Solids Turbulence Characteristics

Particles in the downer and riser are randomly turbulent because of the violent collisions between particles and particles, as well as the gas-solids interaction inside the downer and riser. Granular

temperature is usually used to characterize the solids turbulence and it is evaluated as averaging the square of fluctuating velocity in all three directions as shown in the formula below:

$$\Theta = \frac{1}{3}\left(\overline{u'_{px}u'_{px}} + \overline{u'_{py}u'_{py}} + \overline{u'_{pz}u'_{pz}}\right), \tag{5}$$

The total granular temperature was decomposed into the axial and radial component in order to analyze the axial and radial solids turbulence in detail. The axial and radial granular temperature are defined below:

$$\Theta_{axial} = \frac{1}{3}\overline{u'_{pz}u'_{pz}}, \tag{6}$$

$$\Theta_{radial} = \frac{1}{3}\left(\overline{u'_{px}u'_{px}} + \overline{u'_{py}u'_{py}}\right), \tag{7}$$

Next, the axial distribution of granular temperature in downer and riser is shown in Figure 23. The granular temperature increased with the development of gas-solids flow in the downer, which was in accordance with simulation results by Samruamphianskun et al. [60]. The overall value of the granular temperature in the riser was much higher than that in the downer, which indicated that much more intense solids turbulence existed in the riser. Meanwhile, the axial granular temperature in both the downer and riser was much higher than the radial granular temperature since the axial flow was the main direction and is dominant in both the downer and riser.
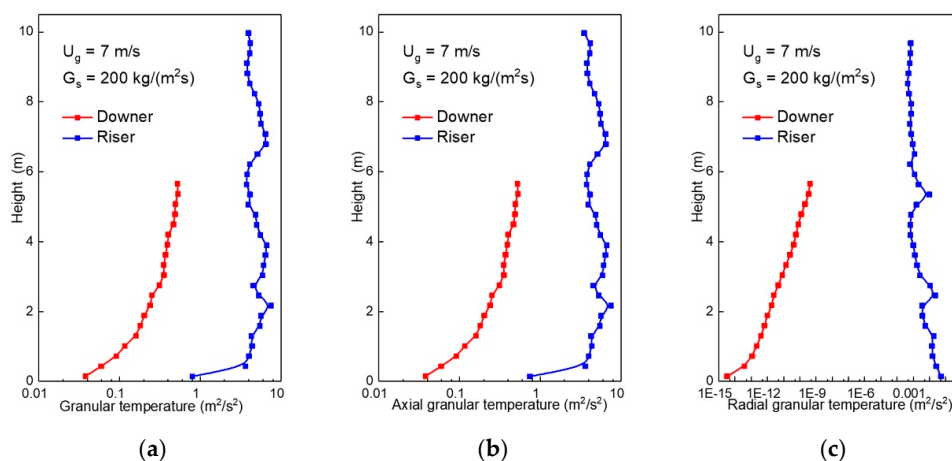

Figure 23. Axial distribution of granular temperature in downer and riser. (**a**) Total granular temperature; (**b**) axial granular temperature; (**c**) Radial granular temperature.

4. Conclusions

In this work, the 3D CPFD model incorporated with the cluster-based and EMMS-based drag model was applied to compare the gas-solids flow characteristics in the CFB downer and riser. Solids holdup and solids velocity, which were two key parameters to reveal the gas-solids flow behaviors, were compared in the downer and riser. In addition, the difference of solids back-mixing behavior was revealed by comparing the cumulative distribution of solids residence time inside the downer and riser. Additionally, the particle scale information such as the solids dispersion and solids turbulence was evaluated by comparing the difference of solids dispersion coefficient distribution and granular temperature distribution inside the downer and riser. From the above comparison, the following conclusions were obtained:

(1)　Compared to the riser, the radial distribution of solids holdup and solids vertical velocity were more uniform in the downer. The overall solids holdup in the riser was higher than that in the downer. Solids vertical velocity in both the downer and riser exhibited higher velocity in the

center and lower velocity near the wall, which is mainly due to the wall friction and due to the frequent formation and dissolution of clusters.

(2) The non-uniformity index for the radial distribution of solids holdup was 0.02 for the downer and ranged between 0.3 and 0.4 for the riser, further demonstrating that the gas-solids flow in downer was much more uniform than that in riser. The higher non-uniformity in the riser was mainly due to the large cluster with vertical strand or "V" shape.

(3) Compared to riser, the cumulative distribution of solids RTD curve displayed a much steeper slope in the downer, which indicated that limited solids back-mixing existed in the downer and the solids flow structure approached to the ideal plug flow.

(4) The axial solids dispersion coefficient in the downer was higher than that in the riser which indicated that solids transportation ability is much stronger in the downer under the same operating conditions. The decrease of axial dispersion coefficient near the wall in the riser was mainly due to the formation of large volume clusters.

(5) The granular temperature in downer was much smaller compared with the riser, which implied that solids turbulence in the downer was much weaker.

Author Contributions: Conceptualization, X.L. and J.G.; methodology, Y.L. and Y.W.; software, Y.L. and Y.W.; experiment, C.W.; formal analysis, Y.L.; data curation, X.S.; writing—original draft preparation, Y.L.; writing—review and editing, X.S. All authors have read and agreed to the published version of the manuscript.

Conflicts of Interest: The authors declare no conflict of interest.

Nomenclature

A	Particle acceleration, m·s^{-2}
C_{d0}	Homogeneous drag coefficient
C_{dcl}	Drag coefficient of cluster
D	Solids dispersion coefficient, m^2/s
D_p	Interphase momentum transfer coefficient, m/s^2
d_p	Individual particle diameter, m
d_{cl}	Equivalent diameter of cluster, m
f	Particle probability distribution function
F_D	Interphase drag force, N
g	Gravitational acceleration, m·s^{-2}
G_s	Solids mass flux, kg·m^{-2}·s^{-1}
H	Height of CFB downer and riser, m
H_D	Heterogeneity index
m_p	Mass of particle, kg
n	Number of particles in the sampled local area
∇p	Pressure gradient of the gas phase, Pa/m
p_g	Gas pressure, Pa
P	Operating pressure of CFB downer and riser, Pa
P_0	Time-averaged pressure at different heights
r	Displacement of particle
Re_{cl}	Cluster Reynold number
Re_p	Particle Reynold number
t	Time, simulation time, s
T_p	Temperature of particle phase, K
u_g	Gas phase velocity, m/s

u_p	Particle phase velocity, m/s
$u_p{}'$	Fluctuating velocity of particles, m/s
U_g	Superficial gas velocity for downer and riser operation, m/s
x_p	Spatial position of the particles
Greek Letters	
ρ_g	Gas density, kg·m^{-3}
ρ_p	Particle density, kg·m^{-3}
τ_g	Gas phase stress tensor
τ_p	Normal stress of particle phase, N·m^{-2}
ε_{cp}	Particle phase volume fraction at close packing
ε_g	Gas phase volume fraction
ε_p	Particle phase volume fraction
ε_{cp}	Particle-phase volume fraction at close packing
β	Interphase drag coefficient, kg/m^3 s
Θ	Granular temperature, m^2/s^2
θ	Dimensionless solids residence time
μ_g	Gas viscosity, kg·m^{-1}·s^{-1}

References

1. Kunii, D.; Levenspiel, O. *Fluidization Engineering*, 2nd ed.; Butterworth Heinemann: Oxford, UK, 1991.
2. Nowak, W.; Mirek, P. 16-Circulating fluidized bed combustion (CFBC). In *Fluidized Bed Technologies for Near-Zero Emission Combustion and Gasification*; Scala, F., Ed.; Woodhead Publishing Series in Energy; Woodhead Publishing Limited: Sawston, UK, 2013; pp. 701–764. [CrossRef]
3. Zhang, H.; Huang, W.; Zhu, J. Gas-solids flow behavior: CFB Riser vs. Downer. *AIChE J.* **2001**, *47*, 2000–2011. [CrossRef]
4. Wu, B.; Zhu, J.; Briens, L. A Comparison of Flow Dynamics and Flow Structure in a Riser and a Downer. *Chem. Eng. Technol.* **2007**, *30*, 448–459. [CrossRef]
5. Li, D.; Ray, M.B.; Ray, A.K.; Zhu, J. A comparative study on hydrodynamics of circulating fluidized bed riser and downer. *Powder Technol.* **2013**, *247*, 235–259. [CrossRef]
6. Cheng, Y.; Wu, C.; Zhu, J.; Wei, F.; Jin, Y. Downer reactor: From fundamental study to industrial application. *Powder Technol.* **2008**, *183*, 364–384. [CrossRef]
7. Shu, Z.; Peng, G.; Wang, J.; Zhang, N.; Li, S.; Lin, W. Comparative CFD Analysis of Heterogeneous Gas–Solid Flow in a Countercurrent Downer Reactor. *Ind. Eng. Chem. Res.* **2014**, *53*, 3378–3384. [CrossRef]
8. Shaikh, A.A.; Al-Mutairi, E.M.; Ino, T. Modeling and Simulation of a Downer-Type HS-FCC Unit. *Ind. Eng. Chem. Res.* **2008**, *47*, 9018–9024. [CrossRef]
9. Zhang, H.; Zhu, J.; Bergougnou. M.A. Hydrodynamics in downflow fluidized beds (1): Solids concentration profiles and pressure gradient distributions. *Chem. Eng. Sci.* **1999**, *54*, 5461–5470. [CrossRef]
10. Zhang, H.; Zhu, J. Hydrodynamics in downflow Fluidized Beds (2): Particle Velocity and Solids Flux Profiles. *Chem. Eng. Sci.* **2000**, *55*, 4367–4377. [CrossRef]
11. Wang, C.; Li, C.; Zhu, J. Axial solids flow structure in a high density gas–solids circulating fluidized bed downer. *Powder Technol.* **2015**, *272*, 153–164. [CrossRef]
12. Wang, C.; Zhu, J.; Lan, X.; Gao, J.; Barghi, S. Radial solids flow structure in high flux gas-solids circulating fluidized bed downers. *Powder Technol.* **2016**, *301*, 848–857. [CrossRef]
13. Ma, Y.; Zhu, J. Experimental study of heat transfer in a co-current downflow fluidized bed (downer). *Chem. Eng. Sci.* **1999**, *54*, 41–50. [CrossRef]
14. Luo, B.; Yan, D.; Ma, Y.; Barghi, S.; Zhu, J. Characteristics of gas–solid mass transfer in a cocurrent downflow circulating fluidized bed reactor. *Chem. Eng. J.* **2007**, *132*, 9–15. [CrossRef]
15. Fan, C.; Zhang, Y.; Bi, X.; Song, W.; Lin, W.; Luo, L. Evaluation of downer reactor performance by catalytic ozone decomposition. *Chem. Eng. J.* **2008**, *140*, 539–554. [CrossRef]
16. Wang, C.; Li, C.; Zhu, J.; Wang, C.; Barghi, S.; Zhu, J. A comparison of flow development in high density gas-solids circulating fluidized bed downer and riser reactors. *AIChE J.* **2015**, *61*, 1172–1183. [CrossRef]

17. Ma, Y.; Zhu, J. Heat Transfer in the Downer and the Riser of a Circulating Fluidized Bed–A Comparative Study. *Chem. Eng. Technol.* **2001**, *24*, 85–90. [CrossRef]
18. Wang, C.; Zhu, J.; Barghi, S. Performance evaluation of high density riser and downer: Experimental study using ozone decomposition. *Chem. Eng. J.* **2015**, *262*, 478–489. [CrossRef]
19. Vaishali, S.; Roy, S.; Mills, P.L. Hydrodynamic simulation of gas–solids downflow reactors. *Chem. Eng. Sci.* **2008**, *63*, 5107–5119. [CrossRef]
20. Liu, W.; Li, H.; Zhu, Q. Modeling the hydrodynamics of downer reactors based on the meso-scale structure. *Powder Technol.* **2017**, *314*, 367–376. [CrossRef]
21. Lan, X.; Xu, C.; Wang, G.; Wu, L.; Gao, J. CFD modeling of gas–solid flow and cracking reaction in two-stage riser FCC reactors. *Chem. Eng. Sci.* **2009**, *64*, 3847–3858. [CrossRef]
22. Zhou, Q.; Wang, J. CFD study of mixing and segregation in CFB risers: Extension of EMMS drag model to binary gas–solid flow. *Chem. Eng. Sci.* **2015**, *122*, 637–651. [CrossRef]
23. Zhang, M.; Chu, K.; Wei, F.; Yu, A. A CFD–DEM study of the cluster behavior in riser and downer reactors. *Powder Technol.* **2008**, *184*, 151–165. [CrossRef]
24. Zhao, Y.; Cheng, Y.; Wu, C.; Ding, Y.; Jin, Y. Eulerian-Lagrangian simulation of distinct clustering phenomena and RTDs in riser and downer. *Particuology* **2010**, *8*, 44–50. [CrossRef]
25. Snider, D.M. An Incompressible Three-Dimensional Multiphase Particle-in-Cell Model for Dense Particle Flows. *J. Comput. Phys.* **2001**, *170*, 523–549. [CrossRef]
26. Lanza, A.; Islam, M.A.; Lasa, H.D. CPFD modeling and experimental validation of gas–solid flow in a down flow reactor. *Comput. Chem. Eng.* **2016**, *90*, 79–93. [CrossRef]
27. Lanza, A.; Lasa, H.D. Scaling-up down flow reactors. CPFD simulations and model validation. *Comput. Chem. Eng.* **2017**, *101*, 226–242. [CrossRef]
28. Wu, Y.; Peng, L.; Qin, L.; Wang, M.; Gao, J.; Lan, X. Validation and application of CPFD models in simulating hydrodynamics and reactions in riser reactor with Geldart A particles. *Powder Technol.* **2018**, *323*, 269–283. [CrossRef]
29. Shi, X.; Sun, R.; Lan, X.; Liu, F.; Zhang, Y.; Gao, J. CPFD simulation of solids residence time and back-mixing in CFB risers. *Powder Technol.* **2015**, *271*, 16–25. [CrossRef]
30. Wu, Y.; Shi, X.; Liu, Y.; Wang, C.; Gao, J.; Lan, X. 3D CPFD simulations of gas-solids flow in a CFB downer with cluster-based drag model. *Powder Technol.* **2019**, in press. [CrossRef]
31. Wang, C. High-density gas-solids circulating fluidized bed riser and downer reactors. Ph.D. Thesis, University of Western Ontario, London, ON, Canada, 2013.
32. Peng, G.; Dong, P.; Li, Z.; Wang, J.; Lin, W. Eulerian simulation of gas–solid flow in a countercurrent downer. *Chem. Eng. J.* **2013**, *230*, 406–414. [CrossRef]
33. Chen, H.; Gu, S.; Li, H. Simulation gas-solid flow in the downer with new structure-based drag model. *Powder Technol.* **2018**, *323*, 163–175. [CrossRef]
34. Hu, S.; Liu, X. A general EMMS drag model applicable for gas-solid turbulent beds and cocurrent downers. *Chem. Eng. Sci.* **2019**, *205*, 14–24. [CrossRef]
35. Li, F.; Song, F.; Benyahia, S.; Wang, W.; Li, J. MP-PIC simulation of CFB riser with EMMS-based drag model. *Chem. Eng. Sci.* **2012**, *82*, 104–113. [CrossRef]
36. Chen, C.; Werther, J.; Heinrich, S.; Qi, H.; Hartge, E.U. CPFD simulation of circulating fluidized bed risers. *Powder Technol.* **2013**, *235*, 238–247. [CrossRef]
37. Wang, M.; Wu, Y.; Shi, X.; Lan, X.; Wang, C.; Gao, J. Comparison of Riser-Simplified, Riser-Only, and Full-Loop Simulations for a Circulating Fluidized Bed. *Processes* **2019**, *7*, 306. [CrossRef]
38. Yan, A.; Zhu, J. Scale-Up Effect of Riser Reactors (1): Axial and Radial Solids Concentration Distribution and Flow Development. *Ind. Eng. Chem. Res.* **2004**, *43*, 5810–5819. [CrossRef]
39. Zhang, M.; Qian, Z.; Yu, H.; Wei, F. The solid flow structure in a circulating fluidized bed riser/downer of 0.42-m diameter. *Powder Technol.* **2003**, *129*, 46–52. [CrossRef]
40. Lin, Q.; Wei, F.; Jin, Y. Transient density signal analysis and two-phase micro-structure flow in gas–solids fluidization. *Chem. Eng. Sci.* **2001**, *56*, 2179–2189. [CrossRef]
41. Zhu, J.; Manyele, S.V. Radial Non-Uniformity Index (RNI) in Fluidized Beds and Multiphase Flow Systems. *Can. J. Chem. Eng.* **2001**, *79*, 203–213. [CrossRef]
42. Lu, X.; Li, S.; Du, L.; Yao, J.; Lin, W.; Li, H. Flow structures in the downer circulating fluidized bed. *Chem. Eng. J.* **2005**, *112*, 23–31. [CrossRef]

43. Gomez, N.; Molina, A. Analysis of the Particle Clustering Phenomenon in the Fluid Catalytic Cracking of Gasoil in a Downer Reactor. *Chem. Eng. Technol.* **2019**, *42*, 1293–1303. [CrossRef]

44. Shaffer, F.; Gopalan, B.; Breault, R.W.; Cocco, R.; Karri, S.B.R.; Hays, R.; Knowlton, T. High speed imaging of particle flow fields in CFB risers. *Powder Technol.* **2013**, *242*, 86–99. [CrossRef]

45. Xu, J.; Zhu, J. Visualization of particle aggregation and effects of particle properties on cluster characteristics in a CFB riser. *Chem. Eng. J.* **2011**, *168*, 376–389. [CrossRef]

46. Liu, H.; Lu, H. Numerical study on the cluster flow behavior in the riser of circulating fluidized beds. *Chem. Eng. J.* **2009**, *150*, 374–384. [CrossRef]

47. Ambler, P.A.; Milne, B.J.; Berruti, F.; Scott, D.S. Residence time distribution of solids in a circulating fluidized bed: Experimental and modelling studies. *Chem. Eng. Sci.* **1990**, *45*, 2179–2186. [CrossRef]

48. Rhodes, M.J.; Zhou, S.; Hirama, T.; Cheng, H. Effects of operating conditions on longitudinal solids mixing in a circulating fluidized bed riser. *AIChE J.* **1991**, *37*, 1450–1458. [CrossRef]

49. Chan, C.W.; Seville, J.P.K.; Parker, D.J.; Baeyens, J. Particle velocities and their residence time distribution in the riser of a CFB. *Powder Technol.* **2010**, *203*, 187–197. [CrossRef]

50. Velden, M.V.D.; Baeyens, J.; Smolders, K. Solids mixing in the riser of a circulating fluidized bed. *Chem. Eng. Sci.* **2007**, *62*, 2139–2153. [CrossRef]

51. Huang, C.; Qian, Z.; Zhang, M.; Wei, F. Solids mixing in a down-flow circulating fluidized bed of 0.418-m in diameter. *Powder Technol.* **2006**, *161*, 48–52. [CrossRef]

52. Zhang, Y.; Lu, C.; Shi, M. Evaluating solids dispersion in fluidized beds of fine particles by gas backmixing experiments. *Chem. Eng. Res. Des.* **2009**, *87*, 1400–1408. [CrossRef]

53. Liu, D.; Chen, X. Lateral solids dispersion coefficient in large-scale fluidized beds. *Combust. Flame.* **2010**, *157*, 2116–2124. [CrossRef]

54. Du, B.; Fan, L.; Wei, F.; Warsito, W. Gas and Solids Mixing in a Turbulent Fluidized Bed. *AIChE J.* **2002**, *48*, 1869–1909. [CrossRef]

55. Thiel, W.; Potter, O. The mixing of solids in slugging gas fluidized beds. *AIChE J.* **1978**, *24*, 561–569. [CrossRef]

56. Avidan, A.; Yerushalmi, J. Solids mixing in an expanded top fluid bed. *AIChE J.* **1985**, *31*, 835–841. [CrossRef]

57. Wei, F.; Cheng, Y.; Jin, Y.; Yu, Z. Axial and lateral dispersion of fine particles in a binary-solid riser. Axial and lateral dispersion of fine particles in a binary-solid riser. *Can. J. Chem. Eng.* **1998**, *76*, 19–26. [CrossRef]

58. Wei, F.; Zhu, J.; Yu, Z.; Chen, W.; Mori, S. Lateral and Axial Mixing of the Dispersed Particles in CFB. *J. Chem. Eng. Jpn.* **1995**, *28*, 506–510. [CrossRef]

59. Chalermsinsuwan, B.; Gidaspow, D.; Piumsomboon, P. In-depth system parameters of transition flow pattern between turbulent and fast fluidization regimes in high solid particle density circulating fluidized bed reactor. *Powder Technol.* **2014**, *253*, 522–536. [CrossRef]

60. Samruamphianskun, T.; Piumsomboon, P.; Chalermsinsuwan, B. Computation of system turbulences and dispersion coefficients in circulating fluidized bed downer using CFD simulation. *Chem. Eng. Res. Des.* **2012**, *90*, 2164–2178. [CrossRef]